Lab on a Chip

ROYAL SOCIETY OF CHEMISTRY

PAPER

View Article Online
View Journal

Cite this: DOI: 10.1039/d6lc00033a

A novel 3D-printed tool for *in vitro* cell interaction studies under flow conditions

Katharina Skoll,[a] Maria Zobl,[a] Elke Heiss,[b] Barbara Braunboeck,[b] Samuel Meerkatz,[a] Franz Radner,[c] Samuel Castonguay,[d] Markus Holzner,[e] Adriana Zbiral,[a] Michael Wirth[a] and Maria Anzengruber *[a]

The interaction of drug formulations with cells is a critical factor in the development of effective therapeutics. Conventional *in vitro* models, such as static horizontal monolayer cultures, often fail to account for key parameters such as sedimentation, flotation or shear stress, which influence the cellular dose and interaction dynamics. In this study, the FlowCube, an *in vitro* platform designed to simulate dynamic flow conditions was used to investigate the impact of motion and cell layer orientation on the cell interaction of various particle formulations. Polymeric nanoparticles, microparticles, and buoyant microcapsules were prepared and characterized for size, stability, and sedimentation behaviour. Cell binding of these particles, along with a dissolved lectin ligand as a model soluble substance, was evaluated using the FlowCube and compared with horizontal multiwell plate experiments. Microparticles exhibited significantly lower cell association with vertically oriented cell layers in the FlowCube than with horizontal monolayers, indicating sedimentation-driven accumulation under static conditions. In contrast, buoyant microcapsules showed enhanced cell interaction in the FlowCube, highlighting the role of density-dependent particle dynamics. Cell association of the soluble ligand and the nanoparticle formulation were rather affected by the induced shear stress. These findings demonstrate the critical role of sedimentation, flotation, and shear stress in drug formulation–cell interactions and highlight the need to incorporate controlled motion and consider cell layer orientation for more reliable, physiologically relevant outcomes. The FlowCube is a versatile and valuable addition to conventional *in vitro* models with the potential to improve the accuracy, reproducibility, and translational relevance of *in vitro* drug formulation studies.

Received 12th January 2026,
Accepted 20th April 2026

DOI: 10.1039/d6lc00033a

rsc.li/loc

Introduction

Cell-based *in vitro* assays are widely used as standard tools in drug formulation testing. Traditionally, these experiments are conducted under static, horizontal conditions in multiwell plates (*e.g.*, 96-well plates), which offer convenience and compatibility with high-throughput screening workflows.[1] The multiwell plate, first described in the mid-1950s, was originally developed to facilitate the analysis of samples available only in small quantities, which were unsuitable for conventional reaction tubes.[2] Since then, it has become an indispensable tool in life science laboratories worldwide due to its versatility, cost-efficiency, and ease of standardization. Despite their widespread use, multiwell plate assays have significant limitations. They lack physiological complexity and fail to account for critical parameters that govern the interaction of drug formulations with cells. Essential aspects such as inter-organ communication, tissue-level interactions, and drug metabolism cannot be replicated in these relatively simple static culture systems.[3–5] Furthermore, the absence of dynamic fluid flow is a major drawback, as shear stress is a fundamental feature of the *in vivo* microenvironment.[6–8]

In recent years, particulate carrier systems have become increasingly important in pharmaceutical research, as they enable targeted interactions with diseased tissue and offer new possibilities for controlling drug release, cellular uptake and improving the stability of active pharmaceutical ingredients.[3,9] A wide variety of such systems has been developed within our group, including nanoparticulate carriers, surface-functionalized microparticles, and protein microcapsules, each characterized by distinct physicochemical properties such as size, density, and surface functionality.[10–12] In the case of

[a] *Department of Pharmaceutical Sciences, Division of Pharm. Technology and Biopharmaceutics, University of Vienna, Josef-Holaubek-Platz 2, 1090 Vienna, Austria. E-mail: maria.anzengruber@univie.ac.at*
[b] *Department of Pharmaceutical Sciences, Division of Pharmacognosy, University of Vienna, Josef-Holaubek-Platz 2, 1090 Vienna, Austria*
[c] *University of Vienna, Vienna, Austria*
[d] *Institute of Environmental Engineering, ETH Zürich, Zurich, Switzerland Biodiversity and Conservation Biology Unit, WSL, Birmensdorf, Switzerland*
[e] *BOKU University, Wasserbau, Hydraulik und Fließgewässerforschung, Am Brigittenauer Sporn 3, 1200 Wien, Austria*

particle-based drug formulations, density differences between particles and the surrounding medium can lead to sedimentation or flotation. These processes alter particle distribution within the well, thereby affecting formulation stability, dosing consistency, and cellular uptake.[13–15] Importantly, the extent of cellular interaction is not solely determined by the nominal dose applied to the cells but rather by the cellular dose, the fraction of particles or drug formulation that actually reaches the cell surface.[16] This distinction is critical, as rapid sedimentation can lead to an overestimation of cytoadhesive capacity by increasing contact frequency, while flotation may result in underestimation due to reduced particle–cell contact.[17,18] Despite these drawbacks, static *in vitro* models remain a cornerstone for the development of drug formulations and investigating cell interactions. Animal models, while capturing systemic complexity, present their own challenges. They are costly, difficult to analyse mechanistically, and raise ethical concerns. Moreover, data obtained from animal studies often translate poorly to human (patho-) physiology.[19] These limitations highlight the need for more representative *in vitro* models that better mimic the *in vivo* environment.[3] Microfluidic-based platforms have emerged as promising tools to bridge this gap, providing physiologically relevant microenvironments for detailed drug testing.[20] However, these systems remain technically demanding, resource-intensive, and often unsuitable for high-throughput applications.[21] Their complexity limits routine use in early-stage screening, where large numbers of drug candidates and formulations must be evaluated.[4]

To address these challenges, we developed the FlowCube, a non-static *in vitro* platform specifically designed to simulate flow conditions. The FlowCube enables controlled fluid flow across adherent cell layers in a vertical position, allowing researchers to assess drug formulation performance under dynamic conditions. Lack of shear stress as well as sedimentation are parameters that can lead to under- or overestimating cell interactions, cellular dosing and targeting efficiency in static assays.[22] In addition, flow dynamics have been shown to profoundly influence cellular behaviour, including cell adhesion, morphology, differentiation, proliferation, and barrier function.[23–27] Many cell types, such as vascular endothelial and epithelial cells, naturally experience fluid shear stress within the body.[28–32] Advanced microfluidic devices have demonstrated that even subtle changes in flow rate or shear gradients can significantly alter cell–particle interactions.[26,33] While such systems provide a wealth of information, they often require specialized expertise and complex setups, limiting their accessibility for routine laboratory use. In contrast, the FlowCube is a user-friendly, robust, and simplified experimental platform designed to incorporate shear stress into cell culture assays. It is not intended to replace either multiwell plates or complex microfluidic models but rather to serve as an intermediate solution. By enabling the incorporation of flow into an otherwise simple assay, the FlowCube facilitates a more physiologically relevant characterization of drug formulations without imposing excessive technical burdens. This approach allows for an efficient down-selection of promising candidates prior to their evaluation in more complex models or animal studies, thereby saving time and resources while supporting the principles of animal welfare.

To validate the capabilities of the FlowCube, we tested a variety of nanoparticle and microparticle suspensions with distinct physicochemical characteristics. These included poly-(lactic-*co*-glycolic acid) (PLGA) nano- and microparticles, as well as floating core–shell microcapsules composed of olive oil cores and human serum albumin shells. Additionally, a fluorescently labelled lectin (wheat germ agglutinin) was used as a soluble targeting ligand to explore ligand–receptor interactions under flow conditions.

Experimental

Materials

The following chemicals were obtained from Sigma Aldrich: 2-(4-(2-hydroxyethyl)-1-piperazinyl)-ethansulfonic acid (HEPES), Roswell Park Memorial Institute 1640 Medium (RPMI-1640 Medium), Dulbecco's modified Eagle medium low glucose (DMEM), poloxamer 407, (fluorescence) human serum albumin (fHSA), poly-vinyl-alcohol (PVA, 87–90% hydrolysed, molecular weight 30 000–70 000 g mol^{-1}), propidium iodide (PI), monensin, Corning® laminin (from mouse, >90% purity), Corning® fibronectin (human origin, >90% purity), poly-L-lysine hydrobromide salt, collagen (bovine achilles tendon, type 1), Corning® 500 mL fetal bovine serum, EU Compliant, South American Source (FBS), L-glutamine, poly-D,L-lactic-*co*-glycolic-acid (PLGA) Resomer® RG 503 H, FluorSave™ mounting medium. 4,4-Difluoro-1,3,5,7,8-pentamethyl-4-bora-3*a*,4*a*-diaza-*s*-indacene (BODIPY™ 493/503) was purchased from ThermoFisher Scientific. Fluorescence labelled wheat germ agglutinin (fWGA, Vector Laboratories) was bought from Szabo Scandic. CellTracker Green (CTG), HOECHST 33342 and phalloidin, CF® 594 Biotium were obtained from Invitrogen (Paisley, UK).

FlowCube – design, production and material

The FlowCube is a cubic incubation chamber specifically designed for conducting cell experiments under dynamic conditions. It has dimensions of 20 × 20 × 19 mm (length × width × height) and can hold four glass coverslips. The chamber was constructed using computer-aided design (CAD) software (Fusion 360, Autodesk, USA). A dedicated bottom well accommodates a magnetic stir bar with dimensions of 2 × 8 mm (Fig. 1). The stirring motion ensures that the coverslips are evenly rinsed with the sample fluid under well-controlled shear motion. A short video of the FlowCube on the stirring station is provided in SI.

The inner structure of the FlowCube is uniform across all four side walls, and specific cut-outs in the side walls function as rails to facilitate the precise positioning of coverslips using tweezers. The FlowCube was fabricated using stereolithography (SLA) 3D printing technology with BioMed Clear resin (Formlabs, 3Dee Store, Vienna, Austria). Additionally, a

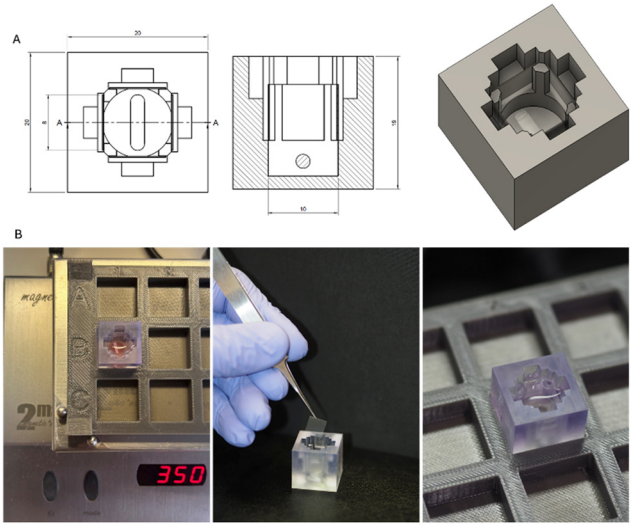

Fig. 1 FlowCube design and geometry (A); FlowCube on the positioning plate on multi-spot magnetic stirrer (B).

positioning plate was designed and 3D printed (material: RS-F2-GPCL-04) to accommodate twelve FlowCubes on a multi-spot magnetic stirring plate (MIXdrive 12 MTP, 2Mag, Munich, Germany). This plate enables easy and centred placement of FlowCubes on individual stirring spots, ensuring consistent experimental conditions across multiple samples. Computational fluid dynamic simulations were performed to characterize the wall shear stress impacting the coverslips.

Cell culture

For cell interaction studies, two cell lines were utilized: 5637 (urothelial bladder carcinoma cells) and HEK293 (human embryonic kidney cells). HEK293 cells exhibit an epithelial morphology and are widely used across various research fields. The 5637 cell line, derived from urothelial bladder carcinoma, is a standard cell line in our laboratory. HEK293 cells were kindly gifted by Prof. Rademacher (University of Vienna), the 5637 cell line was obtained from ATCC (Rockville, USA). Passages between 35 and 54 were used in this study. Compatibility of suspension-grown cells with FlowCube conditions was assessed using THP-1 human monocytes (ATCC, TIB-202). Cells were cultured in RPMI-1640 medium (THP-1, 5637 cells) or DMEM low-glucose medium (HEK293 cells), supplemented with 10% fetal bovine serum (FBS), 0.5 mM L-glutamine, and antibiotics. Cultures were maintained in a humidified atmosphere of 5% CO_2/95% air at 37 °C. HEK293 and 5637 cells were subcultivated at a 1 : 6 ratio using a 0.25% (w/v) trypsin/EDTA solution. THP-1 cells were passaged by centrifugation and resuspension approximately every four days, and cell density was kept within the supplier-recommended range of 0.5×10^6 to 1.5×10^6 cells per ml. For experiments, cells were adjusted to 200 000 cells per ml in RPMI-1640 medium. To evaluate the tolerability of the FlowCube material and stirring conditions, murine monocyte/macrophage J774.1 cells and HepG2 ARE LUC reporter cells were used. J774.1 cells were obtained from ATCC, while HepG2 ARE LUC cells were acquired from Signosis. Both cell lines were maintained in high-glucose DMEM (Sigma), supplemented with 10% FBS, L-glutamine, antibiotics (Invitrogen), in a standard incubator. The J774.1 and HepG2 ARE LUC reporter cell lines were cultured on collagen-coated coverslips. Collagen coating was achieved by incubating the coverslips in a 0.1% (w/v) collagen solution in 0.02 M acetic acid for one hour, followed by thorough rinsing with PBS. Prior to reporter gene assays, HepG2 ARE LUC cells were stained with CellTracker Green (CTG) by incubating them in 10 μM CTG in serum-free medium for one hour. J774.1 and CTG-stained HepG2 ARE LUC cells were seeded onto the coated coverslips placed in appropriate cell culture plates at a density of 100 000–250 000 cells per coverslip. The cells were allowed to attach overnight under static conditions. Subsequently, the coverslips were either transferred to the FlowCube for dynamic experiments or further incubated in conventional culture dishes.

Assessment of cytokine expression by RTqPCR

Coverslips with J774.1 cells were treated with or without lipopolysaccharides (LPS, Sigma; final concentration 100 ng mL^{-1}) under static or stirring conditions. The latter was achieved in the FlowCube with a magnetic bar stirring at a speed of 300 rpm. After 6 hours incubation, total RNA was isolated, reversely transcribed and subjected to qPCR analysis, as previously described in detail.[34] Relative gene expression levels were routinely obtained with the ($2^{-\Delta\Delta Ct}$) method,[35] using the *Ppia* as reference gene (which showed stable expression throughout all treatment conditions). Primer sequences are given in the Table 1 below.

Assessment of Nrf2 activation using a reporter gene assay

Coverslips with CTG-stained HepG2 ARE LUC cells were treated with either dimethyl sulfoxide (DMSO) or a known activator of Nrf2 signaling, CDDO-IM (100 nM; Enzo), under static or stirring conditions. Stirring was performed in the FlowCube equipped with a magnetic stir bar rotating at 300 rpm. After 24 hours of incubation, cells on coverslips were washed with PBS, subjected to one freeze–thaw cycle, and lysed with 50 μL of 1× Promega luciferase lysis buffer (Promega; E1531), supplemented with dithiothreitol (DTT) and coenzyme A under vigorous shaking. Following complete cell lysis, 40 μL of lysate was transferred to a black 96-well plate. Luminescence from firefly

Table 1 Sequences of forward and reversed primers

Gene	Sequence primer
***Il1b**: Sequence fwd primer*	*CAACCAACAAGTGATATTCTCCATG*
***Il1b**: Sequence rev primer*	*GATCCACACTCTCCAGCTGCA*
***Il6**: Sequence fwd primer*	*GAGGATACCACTCCAACAGACC*
***Il6**: Sequence rev primer*	*AAGTGCATCATCGTTGTTCATACA*
***Tnf**: Sequence fwd primer*	*TCTGTCTACTGAACTTCGGGGTGA*
***Tnf**: Sequence rev primer*	*TTGTCTTTGAGATCCATGCCGTT*
***Ppia**: Sequence fwd primer*	*CCAAGACTGAATGGCTGGATG*
***Ppia**: Sequence rev primer*	*TGTCCACAGTCGGAAATGGTG*

luciferase (after injection of luciferin and ATP) and fluorescence from CTG were measured using a TECAN Spark microplate reader. Luminescence values were normalized to fluorescence values to account for potential differences in cell numbers.

Nanoparticle preparation

Poly(lactic-*co*-glycolic acid) (PLGA) nanoparticles were prepared using a solvent-evaporation method with a single oil-in-water (o/w) nanoprecipitation system.[36] Briefly, 50 mg of PLGA RG503H and 25 μg of BodiPy® (as a fluorescent marker for cell adhesion experiments) were dissolved in 2 mL of acetone. This solution was injected *via* syringe (Sterican® 0.60 × 30 mm) into 20 mL of an aqueous solution containing 0.5% (w/v) polyvinyl alcohol (PVA) and sonicated for 2 minutes at 40% amplitude using a Bandelin HD70 Sonopuls sonifier. The mixture was poured into an additional 20 mL of 0.5% (w/v) PVA solution and stirred for 1 hour under continuous airflow to allow acetone evaporation. Nanoparticles were purified through multiple centrifugation steps at increasing *g*-forces for 30 minutes at room temperature. The first pellet (4306 × *g*) was discarded, while subsequent pellets (26 915 × *g*, 47 850 × *g*, 74 766 × *g*, 97 166 × *g*) were pooled and filtered through a 5 μm polycarbonate filter (Whatman Nuclepore). The purified nanoparticle suspension was aliquoted, lyophilized, and stored at 4 °C. All preparation steps were conducted under light protection.

Microparticle preparation

PLGA microparticles were prepared using a modified solvent-evaporation protocol similar to that used for nanoparticles. Fifty milligrams of PLGA polymer and 25 μg of BodiPy® were dissolved in 2 mL of ethyl acetate and injected *via* syringe (Sterican® 0.80 × 40 mm) into 20 mL of 0.5% (w/v) PVA solution. The mixture was emulsified using an IKA UltraTurrax T8 at intensity level 2 for 2 minutes. The dispersion was diluted with an additional 20 mL of 0.5% (w/v) PVA solution and stirred under airflow for solvent evaporation. The particle suspension was washed three times by centrifugation at 5862 × *g* for 15 minutes. The resulting pellet was resuspended in 0.5% (w/v) PVA solution, aliquoted, lyophilized, and stored at 4 °C for further use.

Microcapsule preparation

Microcapsules (MCs) were prepared following a previously established protocol.[37] Twenty milligrams of a 2 : 1 mixture of human serum albumin (HSA) and fluorescently labelled HSA were dissolved in 10 mL of 100 mM phosphate buffer (pH 5.4) and overlaid with 1 mL of olive oil. The probe microtip of a sonifier (Sonopuls HD2070, Bandelin, Germany) was positioned at the interface of the two phases, and the sample was pulse-sonicated at an acoustic power of approximately 253 W cm^{-2} at 100% amplitude for 2 minutes. The resulting microcapsules were washed four times by centrifugation (5204 × *g*, 40 minutes, 4 °C). After each centrifugation step, the microcapsules, which accumulated at the top of the liquid, were separated by removing the lower buffer phase with a syringe. The floating microcapsule pellet was resuspended in 10 mL phosphate buffer containing 1% (w/v) poloxamer 407. For final separation, the capsules were left in a separation funnel at room temperature for 12 hours. The lower aqueous phase containing the capsules was collected for further experiments, while the upper layer containing non-encapsulated olive oil was discarded. Microcapsules were used for cell experiments 2–4 days after preparation.

Particle characterization

Particle size distribution and polydispersity index (PDI) of the nanoparticle suspensions were determined by dynamic light scattering (DLS) using a Zetasizer Nano ZS (Malvern Panalytical, Malvern, UK). The size distribution of microparticles and microcapsules was measured by laser diffraction using a Mastersizer 3000 equipped with a Hydro SV dispersion unit (Malvern Panalytical, Malvern, UK). A laser obscuration rate of 8–12% was applied during measurements, and the particle suspension was stirred at 700 rpm.

Cell interaction studies in multiwell plates and the FlowCube

Cell monolayers were cultivated on pretreated glass coverslips coated with laminin or poly-L-lysine for HEK293 cells or 5637 cells, respectively (SI, Fig. S1). Coverslips were placed in 24-well plates, and 0.5 mL of cell suspension containing 60 000 cells was seeded into each well. Cells were cultured to confluency over three days. Lyophilized PLGA-micro- and nanoparticles were adjusted to a concentration of 0.5 mg mL^{-1} with nutrition medium, the microcapsule formulation was diluted 1 : 5 after the final preparation step, yielding an approximate particle concentration of 0.3–0.4 mg mL^{-1}. The lectin ligand, fluorescence labelled wheat germ agglutinin (fWGA), was used at a concentration of 0.5 μg mL^{-1} for cell experiments. The interaction potential of the prepared formulations was analysed in FlowCube experiments and compared to horizontal monolayer experiments as a reference.

Confluent cell layers on coverslips were rinsed with isotonic HEPES buffer (pH 7.4) and transferred to the FlowCube with the cell layers facing inward. Each FlowCube accommodates four coverslips. As a control, four coverslips were transferred to a separate 24-well plate. Subsequently, 1.2 mL of the respective particle formulation or dissolved fWGA-ligand was added to the FlowCube, while 300 μL of the formulation was added to each coverslip in the 24-well plate. A stir bar was placed in the bottom cavity of the FlowCube to induce gentle shear motion. FlowCubes were placed on a multispot stirring plate and stirring speed was set to 350 rpm. Cell layers in both, the FlowCube with and without stirring, and the 24-well plate were incubated at 37 °C. After incubation times of 1, 2, 4, 8, and 16 hours, coverslips were

transferred to separate 24-well plates and rinsed with buffer. To ensure consistent handling, coverslips incubated in the 24-well plate were also transferred to separate wells for the washing step. Interaction of the particle formulations or lectin ligand with cells was analysed using flow cytometry (Gallios, Beckman Coulter, Brea, CA). Therefore, cells were detached from coverslips using 0.25% (w/v) trypsin/EDTA, suspended in isotonic buffer containing 2% FBS and transferred to flow cytometry tubes. Propidium iodide (PI; final concentration: 3 μM) was added immediately before measurement to differentiate dead cells. Cell-associated fluorescence intensity of the analysed formulations was measured at 488/505–545 nm (excitation/emission), while the PI signal was detected at 561/606–635 nm (ex/em).

The fluorescein molecule used for labelling of the fWGA ligand and fHSA microcapsules is susceptible to pH dependent changes of fluorescence intensity.[38] To account for possible quenching of the fluorescein signal in experiments with these two formulations, cell associated fluorescence intensity was re-analysed after addition of monensin to the cell suspension and incubation for 5 minutes at room temperature. Monensin is an ionophor that elevates the pH of endo-lysosomal compartments and was added at a final concentration of 16 μg ml^{-1}.

Microscopic analysis of cell interaction

HEK293 cells were incubated with the different formulations under static (multiwell plate) and dynamic (FlowCube with stirring) conditions for 16 h. Following incubation, coverslips were transferred to a 24-well plate for staining and imaging. Cell layers were first washed with isotonic HEPES buffer (pH 7.4), and cell nuclei were stained with the DNA-specific dye HOECHST 33342 (12 μg mL^{-1}) for 20 min at 37 °C. After a subsequent wash with isotonic buffer, cells were fixed with 300 μL paraformaldehyde (4% w/v in buffer) for 15 min at 4 °C. Residual aldehydes were quenched by adding 300 μL ammonium chloride (50 mM) for 10 min at room temperature, followed by washing with buffer. Cells were then permeabilized with 200 μL Triton X-100 (0.5% v/v in buffer) for 30 min at 37 °C. The permeabilization solution was removed, and cells were incubated with 200 μl phalloidin working solution (5 U ml^{-1} in 1% BSA) for 30 min at 37 °C to stain F-actin. After a final wash to remove excess dye, coverslips were mounted using FluorSave® mounting medium to preserve fluorescence for imaging.

Fluorescence microscopy was performed on a Zeiss Axio Observer.Z1 epifluorescence microscope (Carl Zeiss, Oberkochen, Germany) and equipped with an HXP-120 light source. Iterative deconvolution was performed using software version ZEN 3.8. For all images a 63x magnification and the following excitation/emission ranges were used: HOECHST 33342-labelled nuclei at 335–383/420–470 nm, phalloidin-red at 530–585/615–4095 nm, and the particle formulations as well as the fWGA ligand at 455–495/505–555 nm. Images of same formulations were acquired using identical exposure settings across conditions (FlowCube *vs.* well plate).

Statistical analysis

Statistical analysis was performed using GraphPad Prism 10. Data sets were tested for normal distribution and analysed using one-way ANOVA (for normally distributed data) with *post hoc* Tukey multiple comparison test or the Kruskal–Wallis test with Dunn's multiple comparison test (for non-normally distributed data). Differences between means were considered statistically significant at * $p < 0.05$.

Results and discussion

Computational fluid dynamics (CFD)

To characterize the flow regime within the FlowCube, we evaluated the Reynolds number using the rotor tip velocity as the characteristic velocity scale and the rotor diameter as the characteristic length scale. At 350 rpm, this yields $Re \approx 1.2 \times 10^3$. This value indicates that inertial effects are significant and exceed viscous forces; the flow is therefore not in a viscous (Stokes) regime. Even though it remains below commonly reported transition thresholds for fully developed turbulence in confined rotating systems, the flow may exhibit transient deviations from the cycle-averaged flow.[39]

To further quantify the hydrodynamic environment, we performed CFD simulations using the exact experimental geometry (Fig. 2A). The rotor region was modelled using a rotating frame of reference (MRF approach) for the steady solution, while the outer chamber was treated in the stationary frame. The fluid was assumed incompressible and Newtonian. Transient simulations were then conducted using a time-dependent formulation with moving mesh to resolve the rotor motion explicitly. Solver convergence was assessed based on residual reduction.

The simulations provide fully resolved three-dimensional velocity fields (Fig. 2B), spatial maps of wall shear stress (WSS) on the cell-seeded plates (Fig. 2C and D), and transient signals of the maximum and average WSS on these plates (Fig. 2E). A video simulating WSS is provided in the SI. Fig. 2B–D correspond to the time instant of peak WSS. At 350 rpm, as shown in Fig. 2C–E, the computed maximum WSS remains below 1 Pa. A shear level of approximately 1 Pa is commonly accepted as the upper physiological threshold for adherent cell cultures.[40–43] The transient analysis did not reveal amplification of peak shear beyond the steady-state predictions. A slight deviation from fully periodic signal is discernible after convergence to a quasi-periodic state, *i.e.* the peak WSS signal weakly still departs from a fully periodic signal after the initial transient ($t > 0.2$ s, Fig. 2E). However, these fluctuations are small, consistent with the moderate Reynolds number of the flow. These results provide a quantitative and reproducible characterization of the hydrodynamic conditions within the FlowCube and confirm that the applied stirring parameters remain within biologically relevant limits.

Next to the design of the FlowCube and the stirring speed also media composition and fluid rheology critically influence the wall shear stress experienced by cells and can therefore alter measured interactions. In this study, we used standard nutrient

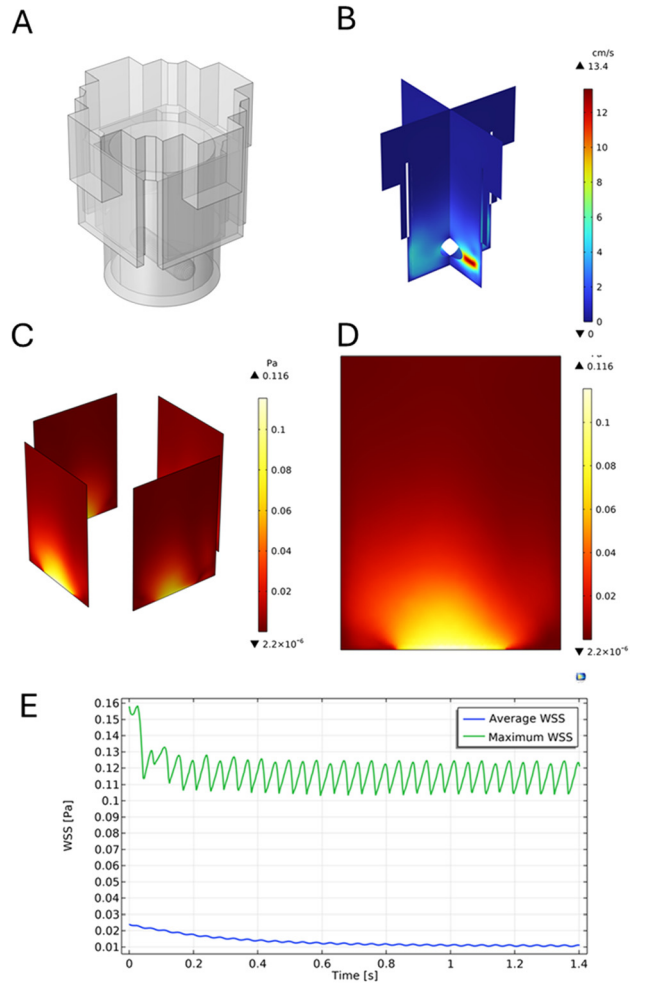

Fig. 2 CFD simulation of wall shear stress in the FlowCube; stirring speed 350 rpm. (2A) geometry of the FlowCube, (2B) three-dimensional velocity fields, (2C and D) map of wall shear stress on cell seeded coverslips, (2E) maximum and average wall shear stress on coverslips.

medium and treated it as a Newtonian fluid, adopting literature values for calculations.[44] While appropriate for comparability and simplicity, this underestimates physiological complexity. Blood is a non-Newtonian fluid and shear-thinning, therefore the apparent viscosity decreases at higher shear rates.[45,46] Consequently, absolute shear stresses and cell responses in our setup may differ from *in vivo* conditions, especially in low-shear regions where blood viscosity increases. Depending on the specific endpoint or experimental design, it may be advantageous to use alternative dispersion media with more "blood-like" viscosity to better mimic *in vivo* rheologic conditions.

FlowCube conditions neither induce a NRF2-dependent stress response nor modulate pro-inflammatory immune signalling

Prior to the examination of FlowCube performance in cell interaction studies, we assessed whether its material and/or the applied shear forces induce or alter stress- or immune signalling in cells. For this, we tested activation of the NRF2 signalling in a reporter gene assay and cytokine expression in murine macrophages, respectively.

HepG2 cells stably expressing a luciferase reporter gene under the control of the antioxidant response element (ARE) were used. This element is typically regulated by transcription factors involved in cellular stress defence, with NRF2 being the primary candidate.[47] When HepG2 ARE LUC cells were exposed to dimethyl sulfoxide (DMSO) as a solvent control or to CDDO-IM, a known activator of NRF2 signalling,[48] basal NRF2 activity (as indicated by luminescence in DMSO-treated samples) was very low and did not differ between static and FlowCube conditions (Fig. 3A). Treatment with CDDO-IM led to a significant induction of luciferase activity; however, the amplitude of this induction was lower under FlowCube conditions (Fig. 3B). These results suggested that cultivation under FlowCube conditions does not elevate basal stress levels in cells. The reduced amplitude of NRF2 activation in the FlowCube warrants further investigation. Possible explanations include impaired uptake or enhanced efflux of CDDO-IM due to stirring, shear-induced modulation of the NRF2 pathway in response to CDDO-IM exposure, or adhesion of the compound to the FlowCube material. As no HEK293 or urothelial cell reporter systems were readily available, HepG2 stress reporter cell lines were used.

This assay was intended to screen for device and flow induced nonspecific stress; no reporter activation was observed under our conditions, indicating minimal baseline perturbation attributable to the FlowCube. Future studies could assess the extent to which cell specific characteristics modulate stress responses in this system.

J774.1 murine macrophages were incubated with or without the proinflammatory stimulus lipopolysaccharide (LPS) under static and stirring conditions. Relative mRNA expression levels of *Il1*, *Il6*, and *Tnf* were analysed. The results indicated that FlowCube conditions did not trigger proinflammatory signalling, as evidenced by the comparable

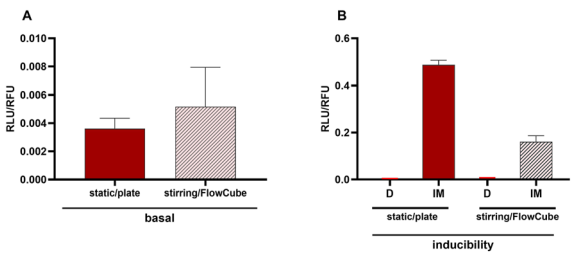

Fig. 3 NRF2-dependent reporter gene expression under static and flow conditions. HepG2-ARE-LUC cells were seeded on collagen coated coverslips before exposing them to medium or medium plus the NRF2 activator CDDO-IM (100 nM) under static and flow conditions. After 24 hours cells were lysed and subjected to luminescence readings as a readout for luciferase expression. (A) Depicts compiled data of DMSO-treated cells from different experiments under static and dynamic conditions. (B) Depicts the compiled data including the readings from CDDO-IM treated cells in both settings. Data shown as mean ± SD (n = 3).

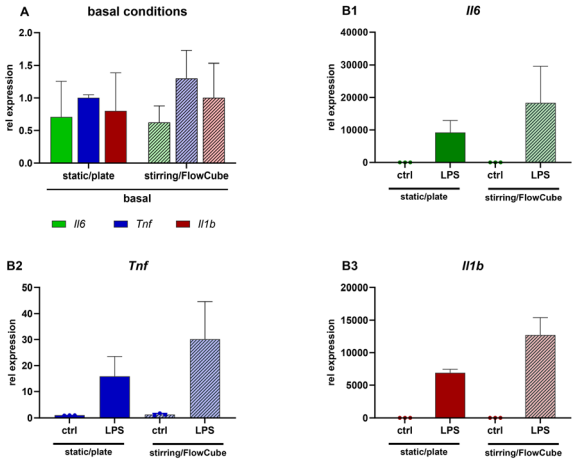

Fig. 4 Expression of proinflammatory cytokines in murine macrophages under static and flow conditions. J774 cells were seeded on collagen-coated coverslips before exposing them to medium or medium plus LPS (100 ng mL^{-1}) under static and flow conditions. After 6 hours RNA was isolated and examined for the relative levels of the indicated cytokines. (A) Depicts compiled data of unstimulated cells from three biological replicates. (B1–B3) depicts the compiled data, including the levels of cytokine mRNA detected after LPS stimulation in both settings. Data shown as mean ± SD (n = 3).

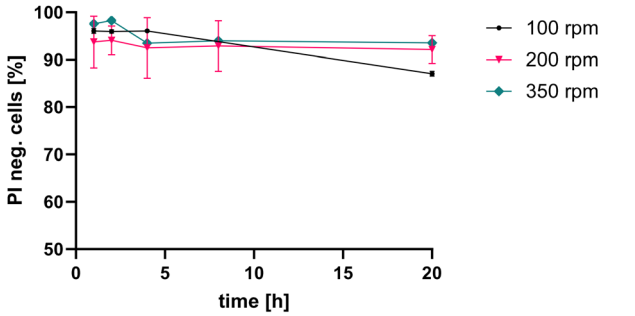

Fig. 5 THP-1 viability in the FlowCube under stirring (100, 200, 350 rpm) for up to 20 h. Viability, indicated by neg. PI staining (3 μM, 5 min), is shown relative to t0 and remained ≥80% at 20 h with a slight reduction at 100 rpm. Data shown as mean ± SD (n = 2).

and low expression levels of these cytokines under both static and stirring control conditions (Fig. 4A). Furthermore, the FlowCube material and shear forces did not inhibit or significantly alter cytokine induction in J774.1 cells upon LPS stimulation (Fig. 4B). Overall, these findings indicate that FlowCube conditions do not trigger any obvious stress or immune response in the accommodated cells.

THP-1 cell viability studies

Analysing cell interaction and behaviour in a physiological context can also involve cells in suspension and exposed to shear forces (*e.g.* circulating immune cells). To assess the suitability of the FlowCube for suspension cultures, THP-1 monocytes were subjected to continuous stirring at 100, 200, or 350 rpm for up to 20 h. Viability was assessed at multiple time points by propidium iodide (PI) staining (3 μM, 5 min). Across all conditions, cell viability remained ≥80% relative to baseline (t_0) after 20 h of incubation, indicating good tolerance to prolonged dynamic exposure (Fig. 5). Notably, cells stirred at 100 rpm showed a modestly higher percentage of PI positive cells than those at 200–350 rpm. A plausible explanation is partial sedimentation at low stirring speeds, increasing contact with the stirrer, whereas higher stirring rates maintained cells in suspension.

Characterization of particle formulations

The functionality and suitability of the FlowCube for *in vitro* cell interaction experiments were evaluated using particle suspensions with distinct physicochemical properties and a fluorescently labelled lectin (fWGA) as a soluble targeting ligand. Polymeric nano- and microparticles were prepared using PLGA as the particle matrix material and BodiPy as a fluorescent dye for tracking. Floating microcapsules were prepared using human serum albumin (HSA) as the shell material and olive oil as the core material.

All particle formulations exhibited narrow size distributions and sufficient stability in the dispersion medium. Polymeric nano- and microparticles were easily dispersible in culture medium after lyophilization, with no signs of agglomeration. The size of PLGA nanoparticles, measured by dynamic light scattering (DLS), was 148 ± 11.0 nm before lyophilization and 142 ± 7.0 nm with a polydispersity index (PDI) < 0.2 after lyophilization. The mean volumetric diameter $D[4;3]$ of PLGA microparticles, determined by laser diffraction, was 17.9 ± 0.72 μm, with $D_x(90)$, $D_x(50)$, and $D_x(10)$ values listed in Table 1. Protein microcapsules were stable for 7–10 days in suspension and were used within 2–4 days post-preparation.[49] However, they exhibited higher batch-to-batch variability regarding size and fluorescence intensity compared to polymeric micro- and nanoparticles. This increased variability can be attributed to the complexity of the preparation protocol, which involves multiple steps and is highly sensitive to minor, unintended variations, ultimately reducing reproducibility. Following the described protocol, microcapsules with a mean volumetric diameter $D[4;3]$ of 1.4 μm were obtained (Table 2). Sedimentation velocities of the respective particles in suspension were calculated using Stokes' equation, assuming densities of 1.3 g cm^{-3} for PLGA particles and 0.96 g cm^{-3} for protein capsules.[50,51]

Cell binding experiments in the FlowCube and multiwell-plate

Binding experiments were conducted using HEK293 and 5637 cells to evaluate the interaction of various formulations with cell layers. Experiments were performed in both the FlowCube (vertical orientation, with or without stirring) and conventional horizontal monolayer setups to compare performance under dynamic *versus* static conditions.

Table 2 Characteristics of particle suspensions used for cell-binding assays ($n \geq 5$)

	HSA-MC	PLGA-MP	PLGA-NP
Mean size	D[4;3] 1.4 μm ± 0.93 μm D_x[90] 2.2 μm ± 0.63 μm D_x[50] 1.0 μm ± 0.08 μm D_x[10] 0.4 μm ± 0.15 μm	D[4;3] 17.9 μm ± 0.72 μm D_x[90] 33.4 μm ± 1.37 μm D_x[50] 16.4 μm ± 0.44 μm D_x[10] 4.30 μm ± 0.69 μm	142 nm ± 7.0 nm PDI 0.14 ± 0.05
Calculated sedimentation velocity	-4.27×10^{-8} m s^{-1}	4.40×10^{-5} m s^{-1}	3.34×10^{-9} m s^{-1}
Density	0.96 g cm^{-3}	1.3 g cm^{-3}	1.3 g cm^{-3}

Nanoparticle binding

Nanoparticulate systems were included because of their relevance to drug delivery and their transport being dominated by diffusion and colloidal stability rather than gravitational settling. Given their size and material density, the formulations remained well dispersed over the incubation period; Brownian motion is expected to outweigh sedimentation under these conditions.[52] Accordingly, no difference in cell association was detected between the static horizontal orientation of the multiwell plates and the static vertical orientation in the FlowCube. Across all conditions, a modest time-dependent increase in cell interaction was observed. When shear stress was introduced, we observed a tendency toward reduced cell association (Fig. 6A). This likely reflects the removal of loosely bound nanoparticles from the cell surface by fluid shear.

Physiologically, shear stress, defined as the tangential stress at the cell–fluid interface, arises not only on endothelial surfaces but also across epithelial interfaces for example in the intestine and kidney.[27,65,70,71] Multiple cell types also modulate endocytic activity in response to shear stress. In epithelial and endothelial cells, shear-dependent increases in membrane tension can impede the initiation of clathrin-coated pits and reduce endocytosis.[53] However, there are cellular mechanisms in place compensating tension-induced suppression of endocytosis. Consistent with such regulation, the density of clathrin-coated pits in renal cells increases upon induction of shear stress.[54,55] Also a close interplay of actin polymerisation with clathrin dependent endocytosis is reported.[56] Thus, flow can potentially alter both, cell binding as well as the rate and route of nanoparticle internalization through biophysical mechanisms.

Further, upon exposure to biological fluids, nanoparticles acquire a protein corona that governs their biological identity and, ultimately, their fate, including biodistribution and cellular interactions.[3,57] The corona is often divided in a tightly bound "hard" layer and a more labile "soft" layer; the latter is dynamic, environment-dependent, and readily exchanged or removed. The composition and structure of the protein corona depend on particle-intrinsic properties (material, size, surface chemistry and charge, hydrophobicity), formulation components (*e.g.*, stabilizers such as PVA or Pluronic),[58] the suspending medium, and the hydrodynamic environment (*e.g.*, shear rate), all of which are directly relevant to the FlowCube experiments.[59,60] Notably, the apparent amount and composition of the corona are also method-dependent: isolation by centrifugation or filtration preferentially retains hard corona constituents, whereas techniques such as asymmetrical flow field-flow fractionation (AF4) can capture aspects of the soft corona.[61] It is reported that dynamic *versus* static incubation primarily affects corona composition,[62] and the total protein load was observed to be moderately higher upon incubation under flow conditions.[25] In this context, the FlowCube could provide a practical platform to analyse how controlled fluid flow modulates nanoparticle–cell interactions both directly, *via* shear-dependent adhesion and endocytosis, and indirectly, by shaping corona composition. Integrating the FlowCube in experiments focusing on protein corona composition could help to clarify how flow conditions influence nanoparticle association with cells.

Microparticle binding

The microparticle system was selected to represent formulations with pronounced sedimentation behaviour, which are expected to lead to elevated local particle accumulation under static conditions and thereby potentially overestimated cellular interaction (Fig. 6B). In the horizontal setup, microparticles rapidly settled onto the cell surface leading to a significantly higher contact probability and, consequently, a greater effective cellular dose. This effect became increasingly evident with longer incubation times, as the gravitational settling of microparticles resulted in cumulative increases in cell-associated fluorescence intensity. After just 1 hour of incubation, the monolayer setup exhibited approximately a 2-fold higher level of cell interaction compared to the FlowCube system. This discrepancy widened substantially over time, and after 16 hours of incubation, in the monolayer setup an almost 10-fold higher cell-associated fluorescence signal relative to the FlowCube was observed.

fWGA-lectin binding

To complement particle-based systems, WGA was included as a soluble ligand to investigate specific carbohydrate-mediated cell interactions.[63] The lectin WGA, possessing high affinity for *N*-acetyl-D-glucosamine and sialic acid, is widely used as a model for studying ligand–cell interactions.[64] In contrast to particulate systems, the use of a soluble ligand allows the investigation of binding processes that are not governed by

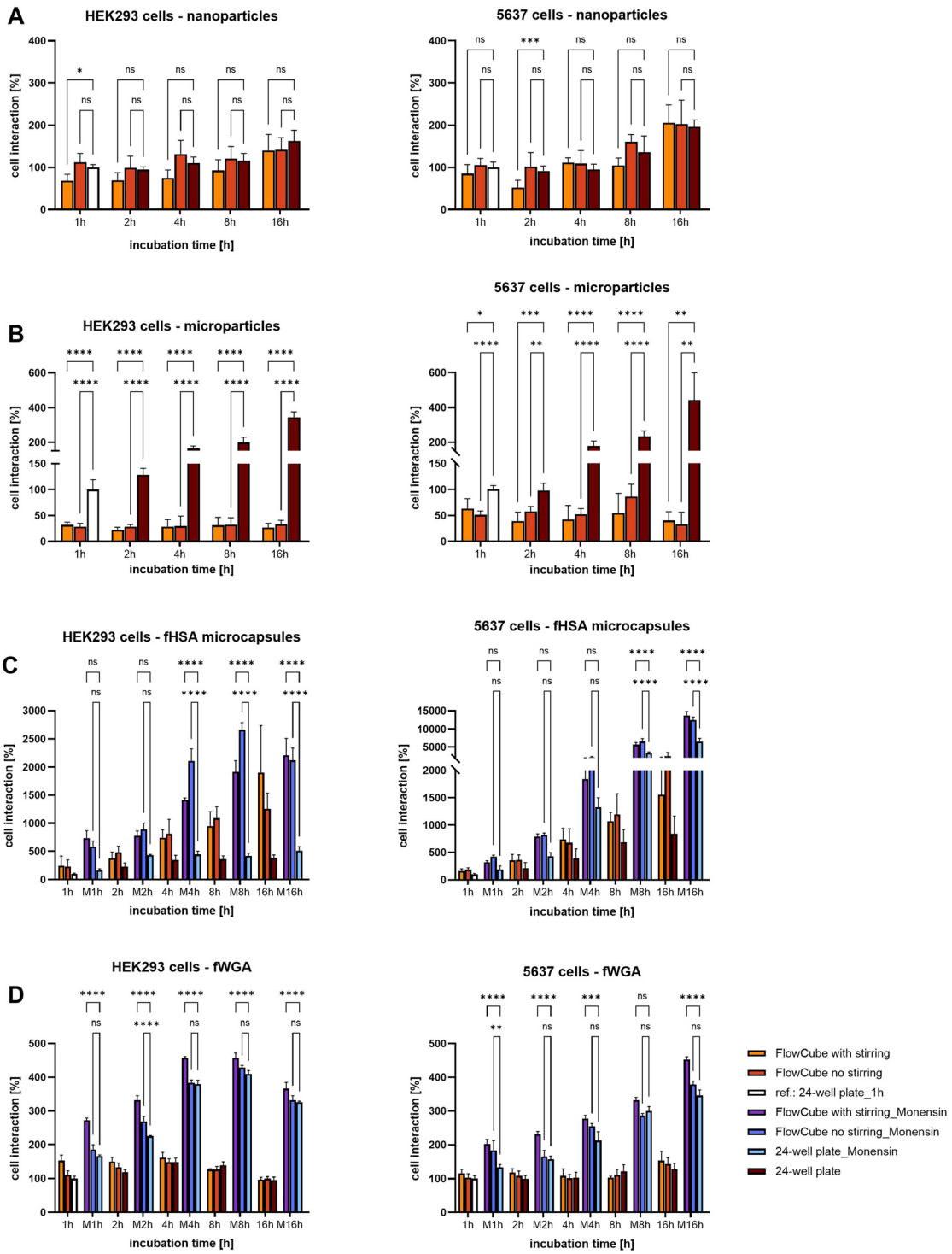

Fig. 6 Cell interaction of nanoparticles (6A, n = 3), microparticles (6B, n = 2), microcapsules (6C, n = 3) and the lectin ligand (6D, n = 3) with 5637 cells (right) and HEK-293 cells (left) in the FlowCube with and without stirring and in a multiwell plate. Results after monensin treatment (purple bars) compared to results prior incubation with monensin are shown in Fig. 5C (fHSA microcapsules) and 5D (fWGA). The determined cell interaction after 1 h incubation of the respective formulation with the cell layer in a 24-well plate was set to 100% and all other results were calculated in reference to this value. This allows for analysing and comparing the interaction behaviour of the respective formulation over time and across experimental setup. Cell interaction was analysed *via* flow cytometry, incubation temperature 37 °C (monensin experiments n = 2) (* $p < 0.05$, ** $p < 0.01$, *** $p < 0.001$, data shown as mean ± SD).

sedimentation or particle transport. This enables a more direct assessment of how dynamic conditions and shear forces influence ligand-mediated interactions at the cell surface.

The dissolved fWGA lectin exhibited minimal differences in cell binding across the experimental conditions, suggesting limited sensitivity to gravitational or flow effects. No consistent trend toward either higher or lower cell interaction was observed among the FlowCube (with or without stirring) and the horizontal multiwell plate setups. Over longer incubation periods, cell-associated fluorescence intensity did not increase but instead either plateaued (5637 cells) or slightly decreased (HEK-293 cells) (Fig. 6D). This decrease may be attributed to reduced interaction, exocytosis of the ligand, or fluorescence quenching in acidic cellular compartments. For fluorescein a pH dependent change of fluorescence intensity has been reported.[38] To further investigate this phenomenon, endo-lysosomal pH was elevated by adding monensin to the cell suspension. After a 5 minute incubation at room temperature, fluorescence intensity was reanalysed. The second measurement revealed a clear increase in cell-associated fluorescence intensity over time, indicating pH-dependent quenching of the fluorescent signal (Fig. 6D). Across all experiments, a minor increase in lectin binding was observed in the stirred FlowCube setup. Although this difference was not statistically significant at every time point, it is noteworthy due to its reproducibility. The underlying cause of this phenomenon is currently under investigation. We hypothesize that it may result from improved distribution of the ligand within the sample, leading to enhanced contact probability with the cell layer, or from alterations in the endocytic behaviour of cells induced by the stirring motion.

Shear stress potentially impacts the abundance and spatial organisation of adhesion receptors and junctional components. It is reported that endothelial cellular adhesion molecules (CAM, *e.g.*, ICAM 1, VCAM 1, PECAM 1) and tight junction proteins (ZO 1, occludin, claudins) undergo shear-dependent changes in expression and clustering.[28,29,65–67] Also, receptor clustering can increase local effective "on-rates" for ligand binding by concentrating binding sites and reducing diffusion constraints, thereby enhancing the stability of multivalent interactions even as global residence time of weakly bound substances and particles decreases under flow. Thus, shear increases the selectivity of binding rather than uniformly increasing or decreasing it.[14,66,68,69]

Since the particle formulations used in this study were not modified with a specific targeting ligand and therefore rely on unspecific adhesions only, this can at least partly explain the reduced cell association observed for nanoparticles under the influence of shear stress. Also, it substantiates the observations made for the ligand WGA which showed higher cell interaction in the dynamic experimental setup. Therefore, including shear stress into the experiment can reveal the full potential of a targeting ligand and using the FlowCube enables this in a simple and standardized manner.

Microcapsule binding

Compared to sinking microparticles, an inverse trend in cell interaction was observed for the microcapsule formulation, which contained a low-density olive oil core. These microcapsules represent buoyant formulations that are expected to exhibit limited particle–cell interactions under conventional static conditions, potentially leading to an underestimation of cell interaction. Albumin-based microcapsules have been previously studied within our working group and were therefore included as a relevant model for these investigations. Unlike microparticles, the microcapsules did not sediment but instead exhibited buoyant behaviour, tending to float away from the cell layer in the horizontal monolayer setup (Fig. 6C). This flotation limited contact between the microcapsules and the cell surface, resulting in low cytoadhesive capacity under standard multiwell plate conditions. In contrast, the vertical FlowCube configuration significantly enhanced cell interaction for the same formulation. This increase aligns with the flotation properties of the microcapsules, as the vertical orientation allowed prolonged contact with the cell layer. Notably, even a modest negative sedimentation velocity (*i.e.*, flotation) was sufficient to substantially reduce particle–cell contact in horizontally oriented static assays. Over time, in both experimental setups an increasing cell interaction was observed; however, the increase in signal intensity and therefore cell interaction was more pronounced in the vertical FlowCube system.

The microcapsule preparations exhibited substantial variability in fluorescence intensities across different batches, leading to inconsistent levels of cell-associated fluorescence intensity as measured by flow cytometry. Consequently, large standard deviations were observed when analyzing results from different experiments without prior normalization. To emphasize on the differences between the FlowCube and multiwell plate experimental conditions, all data were reanalysed and normalized to the cell-associated fluorescence intensity determined for the multiwell plate experiments at each time point (SI, Fig. S2). This normalized data presentation clearly demonstrates a significantly higher level of cell interaction in the FlowCube setup. With respect to the influence of shear stress, no consistent trend applicable to all time points and both cell lines was observed. As for the microparticle formulation analysed in this study, the orientation of the cell layer and consequently the sedimentation or flotation characteristics predominantly determining the observed cell–particle interactions.

Since fluorescein, used for labelling of the albumin microcapsules, exhibits a pH-dependent fluorescence intensity, the microcapsule binding experiments were repeated after elevating endo-lysosomal pH by addition of monensin. Similar to the results observed for the fWGA ligand, a strong increase in cell-associated fluorescence intensity was detected after monensin treatment (Fig. 6C). The overall trend of stronger microcapsule interaction with cells in the vertical orientation remained unchanged. Monensin treatment was not performed for experiments with polymeric nano- and microparticles since the fluorescence intensity of the BodiPy label used is not susceptible to pH changes.

These results underscore the critical role of sedimentation behaviour, static conditions, and incubation times in determining the interaction between drug formulations and cells. They indicate that the dominant determinant of cell association for larger microparticles and microcapsules is gravitational settling or rising, where the sedimentation velocity correlates with particle size and density contrast to the suspension medium. In contrast, for nanoparticles and soluble WGA diffusion and colloidal stability prevail over sedimentation. The observed interaction with cells is therefore rather modulated by shear stress. This highlights the challenges of directly comparing different formulations in static horizontal experiments and emphasizes the importance of incorporating additional parameters, such as fluid flow, cell layer orientation, and various time points, into experimental designs.

In many studies, cellular responses to laminar shear have been characterized in endothelial cells, where sustained physiological shear promotes alignment and elongation in the direction of flow, suppresses proliferation, and induces anti-inflammatory gene expression;[28,72] perturbations, including low or oscillatory shear, can disrupt polarity, increase permeability, and activate inflammatory pathways.[65] In addition, laminar shear is a potent organizer of the cytoskeleton. In endothelial monolayers, shear can redistribute actin filaments into stress fibres aligned with the flow direction, reinforce junctional actin, and promote maturation of focal adhesions and planar cell polarity.[60,73,74] Cellular responses to shear stress rely on complex processes of mechano-sensing and mechano-transduction. Initial detection occurs at the cell membrane, where structures such as the glycocalyx and membrane-associated proteins function as primary mechanosensors.[74,75] Shear stress-induced alterations in membrane fluidity and permeability can then activate intracellular signalling pathways. Furthermore, focal adhesions and integrin-based connections to the extracellular matrix facilitate force transmission and signal amplification, while cytoskeletal remodelling affecting actin filaments, microtubules, and intermediate filaments enables structural adaptation to mechanical stress.[65,74]

In epithelial cells, fluid flow likewise alters morphology and function,[76] with reports of increased monolayer thickness in Caco-2 cultures[70] and accelerated wound closure *via* enhanced migration and proliferation under physiological shear.[77,78] These responses are magnitude- and time-dependent; excessive shear can cause membrane damage and apoptosis.

To assess whether the shear generated in the FlowCube is sufficient to elicit cytoskeletal remodelling, primary HUVECs were incubated for 16 h in the FlowCube with stirring, stained with phalloidin-red, and imaged by fluorescence microscopy (SI). Under stirred conditions, cells exhibited a redistribution of actin into thicker bundles consistent with shear-induced stress fibre formation, whereas unstirred controls retained a more cortical and diffuse actin pattern. These qualitative observations indicate that the FlowCube can produce shear within the biologically relevant regime necessary to trigger endothelial actin filament distribution. Further work should quantify junctional protein organization, the onset kinetics of cytoskeletal reorganization, and the dependence on stirring speed and exposure duration (SI, Fig. S3).

Microscopic analysis of cell interaction

Particle cell interaction was additionally visualised in microscopic imaging studies performed after 16 h of incubation in the dynamic FlowCube and static horizontal setup (Fig. 7). Imaging analysis corroborated the flow cytometric findings. Under conditions favouring sedimentation, microparticle–cell association increased, whereas flotation of microcapsules reduced measurable association. Cell association of nanoparticles was slightly reduced in the dynamic setup and the fWGA ligand–cell interaction was comparable in both setups. These results collectively highlight that sedimentation/flotation and the choice of static *versus* dynamic assay conditions are major determinants of the observed cell–particle association. For cell interaction experiments we did not distinguish between internalised and strongly surface adhered particles, as the experiments were designed to assess unspecific interactions. The images, however, indicate a certain degree of internalisation for nanoparticles and fWGA, larger microparticles as well as microcapsules are mainly located on the surface of the cells. Future work should further clarify the distinctions among endocytosis pathways, as these can be influenced by shear stress.

Impact of experimental setup and incubation time on cell viability

To assess the impact of experimental conditions and incubation time on cell viability, propidium iodide (PI) staining was performed prior to flow cytometry. As a control and to detect possible toxicity originating from the particle formulations or the fWGA-ligand, cells incubated with culture medium alone (no formulation added) in a stirred FlowCube setup were included in the analysis. For both cell lines, the percentage of PI-positive cells did not differ significantly between experimental setups at any time point. HEK-293 cells showed no increase in PI signal over 16 hours (Fig. 8A), while 5637 cells exhibited a time-dependent but not setup-dependent increase in PI-positive cells (Fig. 8B). These results indicate that the vertical orientation and flow conditions in the FlowCube do not negatively affect cell viability within a 16 hour incubation period. PI-positive cells were excluded from further analysis of cell association for the respective formulations.

Does FlowCube data flow with the flow?

This study was designed to compare cell interactions across formulations as a function of the experimental configuration, specifically contrasting static *versus* dynamic incubation and evaluating the contribution of sedimentation to apparent cell association. A further objective was to assess the feasibility of prolonged flow-based assays with adherent cell types.

Consistent with prior *in vitro* studies[15,46,68,69,79–82] using a variety of, sometimes custom made, microfluidic devices as well as mathematical simulations,[13,52,83,84] our results demonstrate

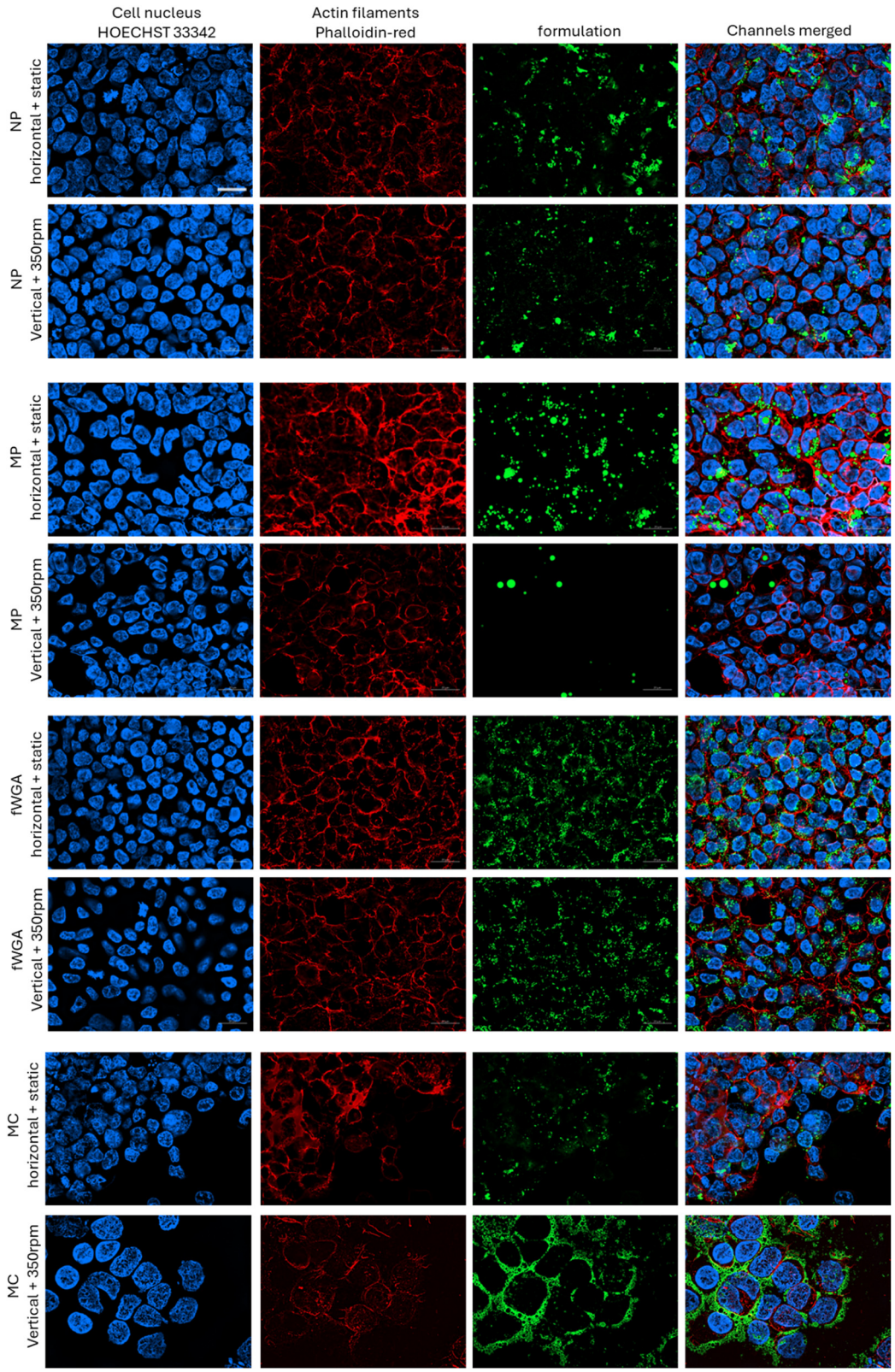

Fig. 7 Visualization of HEK-293 cell interaction with BodiPy labelled nanoparticles (NP), microparticles (MP), fluorescein labelled WGA (fWGA) and fluorescein labelled HSA-microcapsules (MC) (green); HEK-293 cells were incubated for 16 h under horizontal/static or vertical/dynamic (350 rpm) conditions. Nucleus stain HOECHST 33342 (blue), actin filaments stained with phalloidin-red (red), formulation analysed (green). Scale bar indicates 20 μm and applies to all images; 63× magnification.

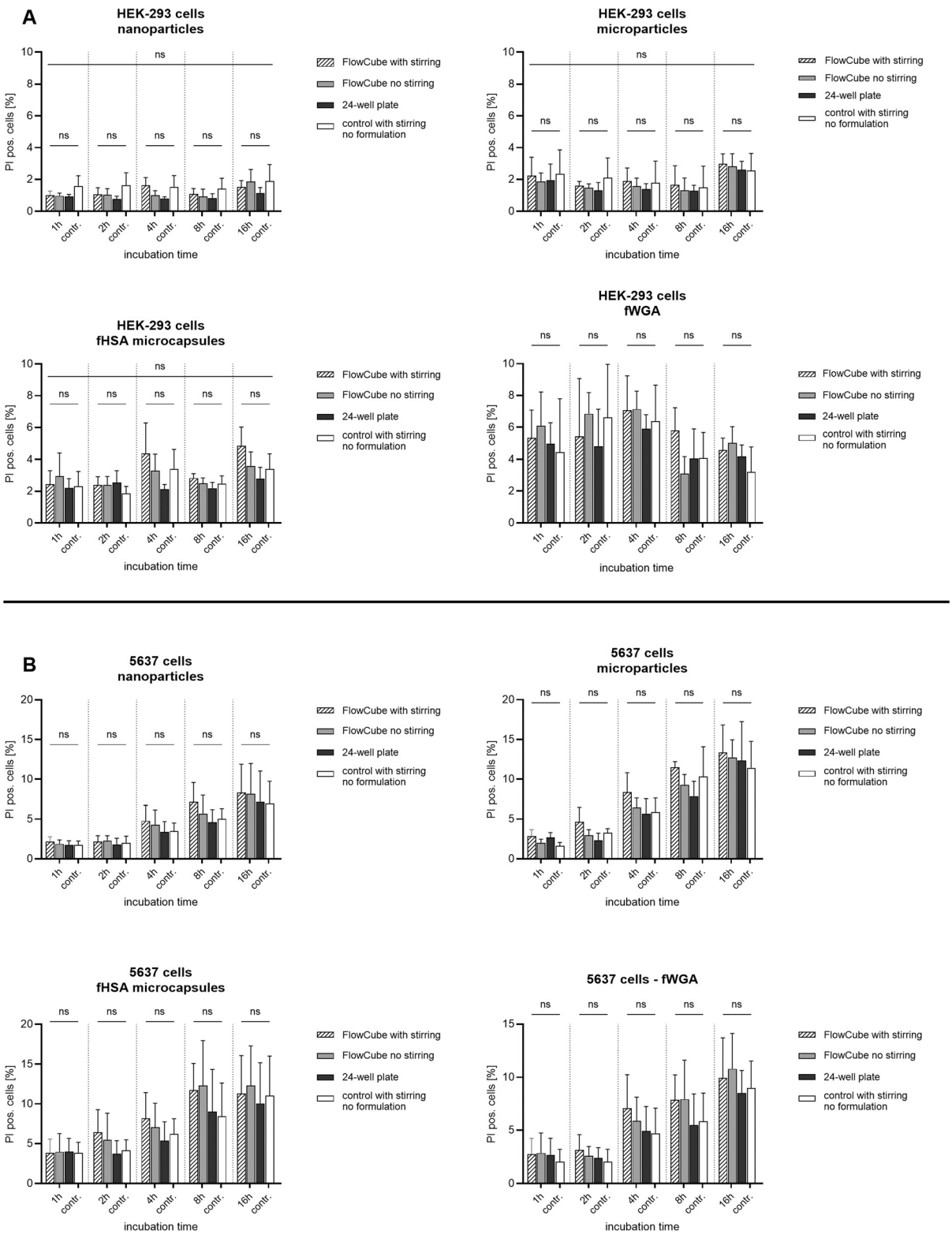

Fig. 8 Cell viability assay. Percentage of PI positive cells analysed by flow cytometry. No statistically significant change in PI pos. cells was observed for HEK-293 cells (8A) and 5637 cells (8B) between experimental setups. 5637 cells show time dependent increase in PI positive cells but no difference between experimental setups (5637 cells: n = 3, HEK-293 cells: n = 2; data shown as mean ± SD).

that the delivered cellular dose is strongly shaped by transport phenomena rather than the nominal media concentration. Even seemingly minor procedural details (*e.g.*, pre-dilution, in-well dilution, pipette angle) can alter the fraction of particles that

reach the cell surface.[79] In static, horizontally oriented cultures, sedimentation increases apparent association; inverting the monolayer or placing it in a vertical orientation diminishes this effect, underscoring the gravitational contribution.[13,15] Dynamic flow reduces sedimentation-driven contact and thereby lowers measured interaction.[46,80] Also, under flow conditions, nonspecific interactions are generally reported to decrease however, targeting ligands retain or enhance relative specificity.[68,69,81,82] Theoretical analyses indicate that particle size and density also modulate how particles are affected by a fluid stream. Smaller and less dense particles are more likely to escape from the fluid stream and impact on surfaces (*e.g.* vessel wall) as compared to larger and heavier particles.[85] Collectively, these observations emphasize the need for accurate dosimetry —quantifying the fraction of a formulation that actually contacts cells over time—when interpreting binding, uptake, toxicity, and targeting performance. Our findings align with this literature and support the conclusion that cellular dose, rather than nominal concentration, is a key determinant of experimental outcome.[13,15]

Conclusions

In this study, a set of particle formulations with distinct physicochemical characteristics was prepared to evaluate the impact of motion and cell layer orientation on cell interaction studies. Comparing results from the FlowCube to multiwell plate in *in vitro* cell experiments revealed that sedimentation dynamics and static experimental conditions critically influence drug formulation–cell interactions.

While hardly any impact of cell layer orientation (vertical *vs.* horizontal) on cell interaction of the soluble ligand fWGA and nanoparticles were observed, the shearing motion did influence the results. For nanoparticles, shear stress resulted in lower cell association as compared to a static experimental setup, most likely due to a removal of unspecific and weakly bound nanoparticles caused by the fluid flow. The specific binding of the fWGA ligand on the other hand was slightly enhanced upon the influence of shear stress. The shearing force impacting on the cell surfaces therefore reduces unspecific, weak interactions while at the same time specific, receptor mediated interactions can be increased thereby potentiating the impact of targeting ligands. Microparticle formulations demonstrated reduced cell association in the vertical FlowCube compared to horizontal monolayers. This reduction reflects the sedimentation-driven accumulation of particles on the cell monolayer under static conditions. In contrast, buoyant microcapsules exhibited enhanced interaction with cells in the FlowCube, highlighting the importance of density-related particle dynamics. Moreover, an incubation-time-dependent increase in cell interaction was observed. For the relatively heavy microparticles, this increase was primarily driven by sedimentation. In contrast, for dissolved ligand molecules, which do not undergo sedimentation, the extended incubation time and therefore contact probability was likely the key factor contributing to the observed increase in cellular uptake.

These findings emphasize that the actual cellular dose is a decisive factor in shaping experimental outcomes. Under static, horizontal conditions this complicates direct comparisons between formulations and limits the reliability of translating *in vitro* findings to *in vivo* contexts. Our results underscore the necessity of incorporating controlled motion into *in vitro* studies and carefully selecting the orientation of the cell layer to ensure more physiologically relevant and interpretable results.

The FlowCube is a rather simple yet powerful tool that enables the efficient assessment of key parameters essential for characterizing drug formulations, including cell binding potential, the influence of sedimentation behaviour, and the effects of shear stress on cyto- or bioadhesion. Results presented in this study highlight the importance of such a tool to advance *in vitro* cell experiments to the next level without requiring large time or cost investments.

Within the landscape of *in vitro* systems for investigating drug/formulation–cell interactions under flow conditions, the FlowCube can be positioned in the gap between static multiwell plate experiments and far more complex microfluidic based *in vitro* assays. Conventional static multiwell plate assays remain widely used due to their simplicity, low cost, and the option for high throughput analysis. However, these systems lack fluid dynamics, and their results are inherently influenced by sedimentation and flotation phenomena, which limit the interpretability and comparability of *in vitro* data. Microfluidic systems in contrast, enable precise control over flow profiles and shear stress, as well as microenvironmental conditions, thereby providing a higher degree of physiological relevance. Nevertheless, their implementation typically requires specialized equipment, increased technical expertise, and is often associated with higher operational costs, which may restrict their applicability in many research laboratories and routine screening workflows. The FlowCube represents an intermediate approach that addresses specific limitations of both systems. By combining vertical orientation of cell layers with controlled fluid motion, it minimizes gravity-driven artefacts while introducing defined shear stress. Importantly, this is achieved within a format that remains compatible with standard laboratory infrastructure and established analytical methods. While the FlowCube does not replicate the full complexity of microfluidic systems, it enables a more controlled and physiologically relevant exposure scenario compared to static assays, without substantially increasing experimental complexity. This balance between experimental control, accessibility, and scalability suggests that the FlowCube may serve as a complementary platform for early-stage screening and comparative evaluation of (particulate-) drug formulations under dynamic conditions.

While this study provides valuable insights into the functionality and usefulness of the FlowCube, further characterization and detailed analysis of fluid dynamics and shear forces are necessary to fully understand its potential. Also, a closer investigation of how the applied shear stress impacts

cellular behaviour such as endocytosis pathways, formation and distribution of tight junction proteins and cellular morphology will be material for further studies. Ongoing work in our laboratory is focused on addressing these aspects. Overall, the FlowCube represents a valuable addition to standard laboratory equipment, offering new opportunities to improve the accuracy, reproducibility, and translational relevance of *in vitro* studies across diverse research domains.

Author contributions

KS, MA conceptualised and designed the study; KS, MA, EH, SC, MH analysed the data and wrote the initial draft of the manuscript; MA, MZ, AZ, BB, SM conducted the experiments; FR improved and constructed the CAD file of the FlowCube; MW provided essential resources and reviewed the manuscript. All authors read and approved the final manuscript.

Conflicts of interest

There are no conflicts to declare. Patent application published October 30, 2025 under publication number WO 2025/224312.

Data availability

Data for this article is available on Phaidra repository at https://phaidra.univie.ac.at/o:2186899.

Supplementary information (SI): SI contains the methods and results of coating coverslips with cell-adhesion-promoting substrates and includes microscopic images of HUVECs cultured under static and dynamic (FlowCube) conditions with phalloidin (red) labelling of F-actin. See DOI: https://doi.org/10.1039/d6lc00033a.

Acknowledgements

We gratefully acknowledge the scientific input and support provided by our colleagues, Maria Lummerstorfer and Ulrich Lächelt throughout this study. We want to thank Maria Kovios for taking pictures and creating the video of the FlowCube and Lea Ann Dailey for connecting us with relevant collaborators and Gian Luca Bello for believing in our idea early on and encouraged us to develop it further.

Notes and references

1 E. Berthier, E. W. K. Young and D. Beebe, Engineers are from PDMS-land, biologists are from polystyrenia, *Lab Chip*, 2012, **12**(7), 1224–1237, DOI: 10.1039/C2LC20982A.

2 G. Y. Takátsy, The Use of Spiral Loops in Serological and Virological Mirco-Methods, *Acta Microbiol. Immunol. Hung.*, 2003, **50**(4), 369–383, DOI: 10.1556/AMicr.50.2003.4.5.

3 S. Berger, M. Berger, C. Bantz, M. Maskos and E. Wagner, Performance of nanoparticles for biomedical applications: The in vitro/in vivo discrepancy, *Biophys. Rev.*, 2022, **3**(1), 0113031–01130324, DOI: 10.1063/5.0073494.

4 F. Zheng, F. Fu, Y. Cheng, C. Wang, Y. Zhao and Z. Gu, Organ-on-a-Chip Systems: Microengineering to Biomimic Living Systems, *Small*, 2016, **12**(17), 2253–2282, DOI: 10.1002/smll.201503208.

5 M. B. Esch, A. S. T. Smith, J. M. Prot, C. Oleaga, J. J. Hickman and M. L. Shuler, How multi-organ microdevices can help foster drug development, *Adv. Drug Delivery Rev.*, 2014, **69–70**, 158–169, DOI: 10.1016/j.addr.2013.12.003.

6 D. Huber, A. Oskooei, X. Casadevall Solvas, A. Demello and G. V. Kaigala, Hydrodynamics in Cell Studies, *Chem. Rev.*, 2018, **118**(4), 2042–2079, DOI: 10.1021/acs.chemrev.7b00317.

7 H. W. Hoyle, C. M. L. Stenger and S. A. Przyborski, Design considerations of benchtop fluid flow bioreactors for bio-engineered tissue equivalents in vitro, *Biomater. Biosyst.*, 2022, **8**, 100063, DOI: 10.1016/j.bbiosy.2022.100063.

8 S. Naskar, V. Kumaran and B. Basu, Reprogramming the Stem Cell Behavior by Shear Stress and Electric Field Stimulation: Lab-on-a-Chip Based Biomicrofluidics in Regenerative Medicine, *Regener. Eng. Transl. Med.*, 2019, **5**(2), 99–127, DOI: 10.1007/s40883-018-0071-1.

9 F. Y. Han, K. J. Thurecht, A. K. Whittaker and M. T. Smith, Bioerodable PLGA-Based Microparticles for Producing Sustained-Release Drug Formulations and Strategies for Improving Drug Loading, *Front. Pharmacol.*, 2016, **7**, 1–11, DOI: 10.3389/fphar.2016.00185.

10 B. Brauner, C. Schuster, M. Wirth and F. Gabor, Trimethoprim-Loaded Microspheres Prepared from Low-Molecular- Weight PLGA as a Potential Drug Delivery System for the Treatment of Urinary Tract Infections, *ACS Omega*, 2020, **5**, 9013–9022, DOI: 10.1021/acsomega.0c00981.

11 K. Skoll, M. Ritschka, S. Fuchs, M. Wirth and F. Gabor, Characterization of sonochemically prepared human serum albumin nanocapsules using different plant oils as core component for targeted drug delivery, *Ultrason. Sonochem.*, 2021, **76**, 105617, DOI: 10.1016/j.ultsonch.2021.105617.

12 M. Anzengruber, L. M. Nepustil, F. Kurtaj, A. Tahir, K. Skoll, H. Sami, M. Wirth and F. Gabor, A Versatile Brij-Linker for One-Step Preparation of Targeted Nanoparticles, *Pharmaceutics*, 2023, **15**(1403), DOI: 10.3390/pharmaceutics15051403.

13 N. Feliu, X. Sun, R. A. Alvarez Puebla and W. J. Parak, Quantitative Particle-Cell Interaction: Some Basic Physicochemical Pitfalls, *Langmuir*, 2017, **33**(27), 6639–6646, DOI: 10.1021/acs.langmuir.6b04629.

14 E. Broda, F. Martina, U. Lächelt, S. Morys, E. Wagner and C. Bräuchle, Assessing potential peptide targeting ligands by quantification of cellular adhesion of model nanoparticles under flow conditions, *J. Colloid Interface Sci.*, 2015, **213**, 79–85, DOI: 10.1016/j.jconrel.2015.06.030.

15 E. C. Cho, Q. Zhang and Y. Xia, The effect of sedimentation and diffusion on cellular uptake of gold nanoparticles, *Nat. Nanotechnol.*, 2011, **6**(6), 385–391, DOI: 10.1038/nnano.2011.58.

16 G. Deloid, J. M. Cohen and T. Darrah, *et al.*, Estimating the effective density of engineered nanomaterials for in vitro dosimetry, *Nat. Commun.*, 2014, **5**, 3514, DOI: 10.1038/ncomms4514.

17 M. Björnmalm, M. Faria, X. Chen, J. Cui and F. Caruso, Dynamic Flow Impacts Cell − Particle Interactions: Sedimentation and Particle Shape Effects, *Langmuir*, 2016, **32**(42), 10995–11001, DOI: 10.1021/acs.langmuir.6b03216.
18 J. Cui, M. Faria and M. Björnmalm, *et al.*, A Framework to Account for Sedimentation and Diffusion in Particle-Cell Interactions, *Langmuir*, 2016, **32**(47), 12394–12402, DOI: 10.1021/acs.langmuir.6b01634.
19 N. B. Robinson, K. Krieger and F. Khan, *et al.*, The current state of animal models in research: A review, *Int. J. Surg.*, 2019, **72**, 9–13, DOI: 10.1016/j.ijsu.2019.10.015.
20 M. Rothbauer, H. Zirath and P. Ertl, Recent advances in microfluidic technologies for cell-to-cell interaction studies, *Lab Chip*, 2018, **18**(2), 249–270, DOI: 10.1039/c7lc00815e.
21 C. Ma, Y. Peng, H. Li and W. Chen, Organ-on-a-Chip: A New Paradigm for Drug Development, *Trends Pharmacol. Sci.*, 2021, **42**(2), 119–133, DOI: 10.1016/j.tips.2020.11.009.
22 A. Da Silva-Candal, T. Brown and V. Krishnan, *et al.*, Shape effect in active targeting of nanoparticles to inflamed cerebral endothelium under static and flow conditions, *J. Controlled Release*, 2019, **309**, 94–105, DOI: 10.1016/j.jconrel.2019.07.026.
23 X. Li, J. Zou, Z. He, Y. Sun, X. Song and W. He, The interaction between particles and vascular endothelium in blood flow, *Adv. Drug Delivery Rev.*, 2024, **207**, 115216, DOI: 10.1016/j.addr.2024.115216.
24 D. T. Jayaram, S. M. Pustulka, R. G. Mannino, W. A. Lam and C. K. Payne, Protein Corona in Response to Flow: Effect on Protein Concentration and Structure, *Biophys. J.*, 2018, **115**(2), 209–216, DOI: 10.1016/j.bpj.2018.02.036.
25 S. Palchetti, D. Pozzi and A. L. Capriotti, *et al.*, Influence of dynamic flow environment on nanoparticle-protein corona: From protein patterns to uptake in cancer cells, *Colloids Surf., B*, 2017, **153**, 263–271, DOI: 10.1016/j.colsurfb.2017.02.037.
26 C. Verdier, C. Couzon, A. Duperray and P. Singh, Modeling cell interactions under flow, *J. Math. Biol.*, 2009, **58**(1–2), 235–259, DOI: 10.1007/s00285-008-0164-4.
27 N. Jung, J. Schreiner, F. Baur, S. Vogel-Kindgen and M. Windbergs, Predicting nanocarrier permeation across the human intestine in vitro: model matters, *Biomater. Sci.*, 2024, **12**, 5775–5788, DOI: 10.1039/d4bm01092b.
28 M. R. Maurya, S. Gupta and J. Y. S. Li, *et al.*, Longitudinal shear stress response in human endothelial cells to atheroprone and atheroprotective conditions, *Proc. Natl. Acad. Sci. U. S. A.*, 2021, **118**(4), 2–9, DOI: 10.1073/pnas.2023236118.
29 B. J. Ballermann, A. Dardik, E. Eng and A. Liu, Shear stress and the endothelium, *Kidney Int. Suppl.*, 1998, **54**(67), 100–108, DOI: 10.1046/j.1523-1755.1998.06720.x.
30 J. Zhou, Y. S. Li and S. Chien, Shear stress-initiated signaling and its regulation of endothelial function, *Arterioscler., Thromb., Vasc. Biol.*, 2014, **34**(10), 2191–2198, DOI: 10.1161/ATVBAHA.114.303422.
31 M. I. Choudhury, Y. Li and P. Mistriotis, *et al.*, Kidney epithelial cells are active mechano-biological fluid pumps, *Nat. Commun.*, 2022, **13**(1), 1–13, DOI: 10.1038/s41467-022-29988-w.
32 S. Wang and Z. Dong, Primary cilia and kidney injury: Current research status and future perspectives, *Am. J. Physiol.*, 2013, **305**(8), 1085–1098, DOI: 10.1152/ajprenal.00399.2013.
33 U. Goreke, A. Gonzales and B. Shipley, *et al.*, Motion blur microscopy: in vitro imaging of cell adhesion dynamics in whole blood flow, *Nat. Commun.*, 2024, **15**(1), 7058, DOI: 10.1038/s41467-024-51014-4.
34 S. Bahiraii, M. Brenner, W. Weckwerth and E. H. Heiss, Sulforaphane impedes mitochondrial reprogramming and histone acetylation in polarizing M1 (LPS) macrophages, *Free Radical Biol. Med.*, 2024, **213**, 443–456, DOI: 10.1016/j.freeradbiomed.2024.01.029.
35 K. J. Livak and T. D. Schmittgen, Analysis of Relative Gene Expression Data Using Real- Time Quantitative PCR and the 2−ΔΔCT Method, *Methods*, 2001, **25**(4), 402–408, DOI: 10.1006/meth.2001.1262.
36 M. Anzengruber, L. Wimmer, R. Szuchar, K. Skoll, M. Wirth and F. Gabor, LogP of N-acyl-gemcitabine and lectin-corona emerge as key parameters in nanoparticulate intravesical cancer therapy, *Eur. J. Pharm. Sci.*, 2023, **180**, 106330, DOI: 10.1016/j.ejps.2022.106330.
37 K. Skoll, J. Palmetzhofer, M. Lummerstorfer, M. Anzengruber, F. Gabor and M. Wirth, Human serum albumin nanoparticles as a versatile vehicle for targeted delivery of antibiotics to combat bacterial infections, *Nanomedicine*, 2023, **50**, 102685, DOI: 10.1016/j.nano.2023.102685.
38 R. Sjöback, J. Nygren and M. Kubista, Absorption and fluorescence properties of fluorescein, *Spectrochim. Acta, Part A*, 1995, **51**(6), 7–21, DOI: 10.1016/0584-8539(95)01421-P.
39 R. Shnapp and M. Holzner, Bubble-induced convection and flow instability in liquid vessels, *J. Fluid Mech.*, 2024, **996**, 1–20, DOI: 10.1017/jfm.2024.712.
40 C. D. Di, L. Y. Wu and L. P. Lee, Dynamic single cell culture array, *Lab Chip*, 2006, **6**(11), 1445–1449, DOI: 10.1039/b605937f.
41 C. D. Di, N. Aghdam and L. P. Lee, Single-Cell Enzyme Concentrations, Kinetics, and Inhibition Analysis Using High-Density Hydrodynamic Cell Isolation Arrays, *Anal. Chem.*, 2006, **78**(14), 4925–4930, DOI: 10.1021/ac060541s.
42 M. Al-Rubeai, R. P. Singh, A. N. Emery, C. Line and C. Maintenance, Cell cycle and cell size dependence of susceptibility to hydrodynamic forces, *Biotechnol. Bioeng.*, 1995, **46**, 88–92, DOI: 10.1002/bit.260460112.
43 M. Al-Rubeai, R. P. Singh, M. H. Goldman and A. N. Emery, Death Mechanisms of Animal Cells in Conditions of Intensive Agitation, *Biotechnol. Bioeng.*, 1995, **45**(6), 463–472, DOI: 10.1002/bit.260450602.
44 C. Poon and B. Engineering, Measuring the density and viscosity of culture media for optimized computational fluid dynamics analysis of in vitro devices, *J. Mech. Behav. Biomed. Mater.*, 2022, **126**, 105024, DOI: 10.1016/j.jmbbm.2021.105024.
45 Y. I. Cho, D. J. Cho and R. S. Rosenson, Endothelial Shear Stress and Blood Viscosity in Peripheral Arterial Disease, *Curr. Atheroscler. Rep.*, 2014, **16**(404), 1–10, DOI: 10.1007/s11883-014-0404-6.

46 C. Grabinski, M. Sharma, E. Maurer, C. Sulentic, R. M. Sankaran and S. Hussain, The effect of shear flow on nanoparticle agglomeration and deposition in in vitro dynamic flow models, 2015, 5390, 1–10, DOI: 10.3109/17435390.2015.1018978.

47 C. Tonelli, C. C. Iok In and D. A. Tuveson, Transcriptional Regulation by Nrf2, *Antioxid. Redox Signaling*, 2018, **29**(17), 1727–1745, DOI: 10.1089/ars.2017.7342.

48 K. Liby, T. Hock and M. M. Yore, *et al.*, The Synthetic Triterpenoids, CDDO and CDDO-Imidazolide, Are Potent Inducers of Heme Oxygenase-1 and Nrf2 / ARE Signaling, *Cancer Res.*, 2005, **65**(11), 4789–4798, DOI: 10.1158/0008-5472.CAN-04-4539.

49 K. Skoll, M. Ritschka, S. Fuchs, M. Wirth and F. Gabor, Characterization of sonochemically prepared human serum albumin nanocapsules using different plant oils as core component for targeted drug delivery, *Ultrason. Sonochem.*, 2021, **76**, 105617, DOI: 10.1016/j.ultsonch.2021.105617.

50 M. M. Arnold, E. M. Gorman, L. J. Schieber, E. J. Munson and C. Berkland, NanoCipro encapsulation in monodisperse large porous PLGA microparticles, *J. Controlled Release*, 2007, **121**, 100–109, DOI: 10.1016/j.jconrel.2007.05.039.

51 J. A. Jamison, K. M. Krueger and C. T. Yavuz, *et al.*, Size-dependent sedimentation properties of nanocrystals, *ACS Nano*, 2008, **2**(2), 311–319, DOI: 10.1021/nn700144m.

52 B. Uma, T. N. Swaminathan, R. Radhakrishnan, D. M. Eckmann and P. S. Ayyaswamy, Nanoparticle Brownian motion and hydrodynamic interactions in the presence of flow fields, *Phys. Fluids*, 2011, **23**(7), 1–15, DOI: 10.1063/1.3611026.

53 J. G. Joseph and A. P. Liu, Mechanical Regulation of Endocytosis: New Insights and Recent Advances, *Adv. Biosyst.*, 2020, **4**(5), 1–15, DOI: 10.1002/adbi.201900278.

54 B. J. Ballermann, A. Dardik, E. Eng and A. Liu, Shear stress and the endothelium, *Kidney Int. Suppl.*, 1998, **54**, 100–108, DOI: 10.1046/j.1523-1755.1998.06720.x.

55 V. Raghavan, Y. Rbaibi, N. M. Pastor-soler, M. D. Carattino and O. A. Weisz, Shear stress-dependent regulation of apical endocytosis in renal proximal tubule cells mediated by primary cilia, *Proc. Natl. Acad. Sci. U. S. A.*, 2014, **111**(23), 8506–8511, DOI: 10.1073/pnas.1402195111.

56 S. Boulant, C. Kural, J. C. Zeeh, F. Ubelmann and T. Kirchhausen, Actin dynamics counteract membrane tension during clathrin-mediated endocytosis, *Nat. Cell Biol.*, 2011, **13**(9), 1124–1132, DOI: 10.1038/ncb2307.

57 N. J. Braun, M. C. Debrosse, S. M. Hussain and K. K. Comfort, Modification of the protein corona – nanoparticle complex by physiological factors, *Mater. Sci. Eng., C*, 2016, **64**, 34–42, DOI: 10.1016/j.msec.2016.03.059.

58 A. Lins, L. Keuter, D. Mulac, H u. Humpf and K. Langer, Are stabilizers, located on the surface of PLGA nanoparticles, able to modify the protein adsorption pattern?, *Int. J. Pharm.*, 2025, 674, DOI: 10.1016/j.ijpharm.2025.125488.

59 H. Spreen, M. Behrens, D. Mulac, H u. Humpf and K. Langer, Identification of main influencing factors on the protein corona composition of PLGA and PLA nanoparticles, *Eur. J. Pharm. Biopharm.*, 2021, **163**, 212–222, DOI: 10.1016/j.ejpb.2021.04.006.

60 G. Bashiri, M. S. Padilla, K. L. Swingle, M. J. Mitchell, K. Wang and S. J. Shepherd, Nanoparticle protein corona: from structure and function to therapeutic targeting, *Lab Chip*, 2023, **23**, 1432–1466, DOI: 10.1039/d2lc00799a.

61 C. Weber, S. Morsbach and K. Landfester, Possibilities and Limitations of Different Separation Techniques for the Analysis of the Protein Corona, *Angew. Chem., Int. Ed.*, 2019, **58**(37), 12787–12794, DOI: 10.1002/anie.201902323.

62 D. Pozzi, G. Caracciolo and L. Digiacomo, *et al.*, The biomolecular corona of nanoparticles in circulating biological media, *Nanoscale*, 2015, **7**(33), 13958–13966, DOI: 10.1039/c5nr03701h.

63 C. M. Pichl, B. D. Austria, B. Brauner, F. Gabor, M. Wirth and L. Neutsch, Biomimickry of UPEC cytoinvasion: A novel concept for improved drug delivery in UTI, *Pathogens*, 2016, **5**(1), 1–5, DOI: 10.3390/pathogens5010016.

64 L. Neutsch, V. E. Plattner and S. Polster-Wildhofen, *et al.*, Lectin mediated biorecognition as a novel strategy for targeted delivery to bladder cancer, *J. Urol.*, 2011, **186**(4), 1481–1488, DOI: 10.1016/j.juro.2011.05.040.

65 J. A. Espina, M. H. Cordeiro, M. Milivojevic, I. Pajic and E. H. Barriga, Response of cells and tissues to shear stress, *J. Cell Sci.*, 2023, **136**, 1–11, DOI: 10.1242/jcs.260985.

66 M. Godoy-Gallardo, P. K. Ek, M. M. T. Jansman, B. M. Wohl and L. Hosta-Rigau, Interaction between drug delivery vehicles and cells under the effect of shear stress, *Biomicrofluidics*, 2015, **9**(5), 1–19, DOI: 10.1063/1.4923324.

67 C. Verdier, C. Couzon, A. Duperray and P. Singh, Modeling cell interactions under flow, *J. Math. Biol.*, 2009, **58**(1–2), 235–259, DOI: 10.1007/s00285-008-0164-4.

68 T. Kang, C. Park, J. s. Choi, J. h. Cui and B. j. Lee, Effects of shear stress on the cellular distribution of polystyrene nanoparticles in a biomimetic microfluidic system, *J. Drug Delivery Sci. Technol.*, 2016, **31**, 130–136, DOI: 10.1016/j.jddst.2015.12.001.

69 O. C. Farokhzad, A. Khademhosseini and S. Jon, *et al.*, Microfluidic System for Studying the Interaction of Nanoparticles and Microparticles with Cells biomedical applications ranging from imaging to drug, *Anal. Chem.*, 2005, **77**(17), 5453–5459, DOI: 10.1021/ac050312q.

70 L. C. Delon, Z. Guo and A. Oszmiana, *et al.*, A systematic investigation of the effect of the fluid shear stress on Caco-2 cells towards the optimization of epithelial organ-on-chip models, *Biomaterials*, 2019, **225**, 119521, DOI: 10.1016/j.biomaterials.2019.119521.

71 M. Jobst, M. Hossain, E. Kiss, J. Bergen, D. Marko and G. Del Favero, Autophagy modulation changes mechano-chemical sensitivity of T24 bladder cancer cells, *Biomed. Pharmacother.*, 2024, **170**, 115942, DOI: 10.1016/j.biopha.2023.115942.

72 B. Wojciak-Stothard and A. J. Ridley, Shear stress – induced endothelial cell polarization is mediated by Rho and Rac but not Cdc42 or PI 3-kinases, *J. Cell Biol.*, 2003, **161**(2), 429–439, DOI: 10.1083/jcb.200210135.

73 S. Noria, F. Xu, S. Mccue, M. Jones, A. I. Gotlieb and B. L. Langille, Assembly and Reorientation of Stress Fibers Drives Morphological Changes to Endothelial Cells Exposed to Shear Stress, *Am. J. Pathol.*, 2004, **164**(4), 1211–1223, DOI: 10.1016/S0002-9440(10)63209-9.

74 M. Inglebert, L. Locatelli and D. Tsvirkun, The effect of shear stress reduction on endothelial cells: A microfluidic study of the actin cytoskeleton, *Biomicrofluidics*, 2020, **14**(2), 1–8, DOI: 10.1063/1.5143391.

75 M. Y. Pahakis, J. R. Kosky, R. O. Dull and J. M. Tarbell, The role of endothelial glycocalyx components in mechanotransduction of fluid shear stress, *Biochem. Biophys. Res. Commun.*, 2007, **355**(1), 228–233, DOI: 10.1016/j.bbrc.2007.01.137.

76 C. A. M. Fois, A. Schindeler, P. Valtchev and F. Dehghani, Dynamic flow and shear stress as key parameters for intestinal cells morphology and polarization in an organ - on - a - chip model, *Biomed. Microdevices*, 2021, 1–12, DOI: 10.1007/s10544-021-00591-y.

77 M. L. C. Albuquerque, C. M. Waters and U. Savla, *et al.*, Shear stress enhances human endothelial cell wound closure in vitro, *Am. J. Physiol.*, 2000, **279**(1), 293–302, DOI: 10.1152/ajpheart.2000.279.1.H293.

78 S. Molladavoodi, M. Robichaud, D. Wulff and M. Gorbet, Corneal epithelial cells exposed to shear stress show altered cytoskeleton and migratory behaviour, *PLoS One*, 2017, **12**(6), 1–16, DOI: 10.1371/journal.pone.0178981.

79 T. L. Moore, D. A. Urban and L. Rodriguez-Lorenzo, *et al.*, Nanoparticle administration method in cell culture alters particle-cell interaction, *Sci. Rep.*, 2019, **9**(1), 1–9, DOI: 10.1038/s41598-018-36954-4.

80 M. Björnmalm, M. Faria, X. Chen, J. Cui and F. Caruso, Dynamic Flow Impacts Cell-Particle Interactions: Sedimentation and Particle Shape Effects, *Langmuir*, 2016, **32**(42), 10995–11001, DOI: 10.1021/acs.langmuir.6b03216.

81 E. Broda, F. M. Mickler, U. Lächelt, S. Morys, E. Wagner and C. Bräuchle, Assessing potential peptide targeting ligands by quantification of cellular adhesion of model nanoparticles under flow conditions, *J. Controlled Release*, 2015, **213**, 79–85, DOI: 10.1016/j.jconrel.2015.06.030.

82 C. Fillafer, G. Ratzinger and J. Neumann, *et al.*, An acoustically-driven biochip – impact of flow on the cell-association of targeted drug carriers, *Lab Chip*, 2009, **9**(19), 2745–2860, DOI: 10.1039/b906006e.

83 G. Deloid, J. M. Cohen and T. Darrah, *et al.*, Estimating the effective density of engineered nanomaterials for in vitro dosimetry, *Nat. Commun.*, 2014, **5**, 1–10, DOI: 10.1038/ncomms4514.

84 J. G. Teeguarden, P. M. Hinderliter, G. Orr, B. D. Thrall and J. G. Pounds, Particokinetics in vitro: Dosimetry considerations for in vitro nanoparticle toxicity assessments, *Toxicol. Sci.*, 2007, **95**(2), 300–312, DOI: 10.1093/toxsci/kfl165.

85 R. Toy, E. Hayden, C. Shoup, H. Baskaran and E. Karathanasis, Effect of Particle Size, Density and Shape on Margination of Nanoparticles in Microcirculation, *Nanotechnology*, 2011, **22**(11), 1–18, DOI: 10.1088/0957-4484/22/11/115101.

